Chaotic Synchronization between Coupled Pancreatic β-Cells

Brian Lading, Erik Mosekilde, Sergiy Yanchuk* and Yuri Maistrenko*

Center for Chaos and Turbulence Studies, Department of Physics
Technical University of Denmark, 2800 Kgs. Lyngby, Denmark
**Institute of Mathematics, National Academy of Sciences*
Kiev, Ukraine 252601, Russia

The paper first describes the main bifurcation structure for a typical model of an insulin producing pancreatic β-cell. Considering a system of two coupled identical and chaotically spiking β-cells, the paper continues to examine the bifurcations through which low periodic orbits embedded in the synchronized chaotic state lose their transverse stability and produce the characteristic picture of locally and globally riddled basins of attraction. We discuss the different types of riddled basins with the associated phenomena of attractor bubbling and on-off intermittency.

§1. Introduction

There is experimental evidence to show that the insulin producing β-cells of the pancreas can synchronize their behavior such that not only the transitions between the silent and the active phases (the bursts), but also the individual spikes (during the bursting phase) occur simultaneously.[1),2)] Interaction between the cells arises through the diffusive exchange of ions via gap junctions, and a number of workers have investigated how this mechanism can produce synchronization in a system of periodically bursting cells.[3),4)] The β-cells can also exhibit chaotic oscillations.[5),6)] This will typically occur in the transitions between the various bursting states and between bursting and continuous spiking, and it is clearly of biological interest to understand the possible phenomena that can arise from shifts between different types of synchronous and asynchronous chaotic behavior.

Systems of coupled identical chaotic oscillators may attain a state of complete synchronization in which both the phases and the amplitudes develop in precisely the same manner.[7),8)] Partial synchronization[9)] (or clustering[10)]), where some of the oscillators synchronize and others do not, may be observed for systems of three or more interacting chaotic oscillators. An interesting problem relates to what happens when the synchronization breaks down. Another important question concerns the stability of the synchronized state to desynchronizing perturbations in the form of noise or of a small parameter mismatch between the interacting oscillators. Recent studies of these problems have led to the observation of a variety of new phenomena, including riddled basins of attraction,[11),12)] attractor bubbling,[13)] and on-off intermittency.[14),15)]

Riddled basins of attraction are observed in regions of parameter space where the synchronized chaotic state is attracting on the average (the largest transverse Lyapunov exponent is negative), while at the same time particular orbits embedded in the chaotic set are transversely unstable.[11),12)] The basin of attraction for

the synchronized chaotic state may then become a fat fractal, riddled with initial conditions from which the trajectories approach other asymptotic states or diverge to infinity. The transition in which the first orbit in the chaotic set becomes transversely unstable is referred to as the riddling bifurcation. The transition in which the chaotic set loses its average attraction is the blowout bifurcation.

However, destabilization of orbits embedded in the chaotic set is not enough for an observable riddling to arise. This will depend on the global dynamics of the system away from the synchronization manifold. In a series of papers [16)-18)] we have established a detailed description of these phenomena for a system of two coupled logistic maps, emphasizing in particular the distinction between sub- and supercritical riddling bifurcations and the roles of the so-called absorbing and mixed absorbing areas. Attractor bubbling arises in the presence of noise (or of a small parameter mismatch), if the absorbing area still exists after the riddling bifurcation and there are no other attracting states within this area. On-off intermittency can be observed if these restraints on the global dynamics persist after the blowout bifurcation has occurred.

We have recently considered chaotic synchronization and riddled basins of attraction for a system of two coupled Rössler oscillators. [19)] This investigation applied a Lyapunov function approach and a calculation of the largest transverse Lyapunov exponent to establish the sufficient, respectively the necessary condition for synchronization. We also showed how a small parameter mismatch between the interacting oscillators can lead to a shift of the synchronized chaotic state away from the synchronization manifold and to a particular form of intermittent bursting out of synchronization. Similar problems have been considered, for instance, by Rul'kov et al. [20)] and by Johnson et al. [21)] Rosenblum et al. [22)] have shown how one can characterize the resulting state of phase synchronization, and Astrakhov et al. [23)] have analyzed the bifurcations that occur with increasing parameter mismatch as phase synchronization is lost.

The purpose of the present study is to extend the analysis of coupled oscillators to a system of two coupled chaotically spiking pancreatic β-cells. First, however, we use standard continuation techniques to examine the bifurcation structure of a model of the single β-cell and determine the region in two-dimensional parameter space where chaotic dynamics occurs. This study reveals that the transitions between different periodically bursting states (the so-called period-adding transitions) are discontinuous and involve a set of slightly overlapping subcritical period-doubling and saddle-node bifurcations.

We continue the study by examining the bifurcations through which low periodic orbits embedded in the synchronized chaotic state lose their transverse stability and produce the characteristic phenomena of locally and globally riddled basins of attraction, attractor bubbling and on-off intermittency. The destabilization of low-periodic orbits takes place via transverse Hopf bifurcations as well as via transverse pitchfork and period-doubling transitions. For time-continuous systems, the concept of an absorbing area (derived from the theory of non-invertible maps [24)]) no longer applies. However, the existence of trapping zones still appears to play an important role for the global dynamics. These zones are regions of phase space, that are

bounded by unstable manifolds of saddle cycles situated outside the synchronization manifold.

§2. The single-cell model

For many cell types the membrane is excitable, or the membrane potential exhibits complicated patterns of slow and fast oscillations associated with variations in the ionic currents across the membrane. An interesting feature of the β-cell is that its electrical activity usually exhibits a bursting dynamics with alternations between an active (or spiking) state and a silent state. Models of this type of behavior are usually based on the Hodgkin-Huxley equations for neuronal activity [25] with elaborations to account, for instance, for the intracellular storage of Ca^{2+}, for the metabolism of glucose, or for various hormonal signals. Over the years, many such models have been proposed with varying degree of detail. [2-6] Mathematically the models all appear to belong to the same class. Hence, we shall restrain our analysis to consider the following minimal model suggested by Sherman: [3]

$$\begin{aligned} \tau \frac{dV}{dt} &= -I_{\mathrm{Ca}}(V) - I_{\mathrm{K}}(V,n) - g_S(V - V_{\mathrm{K}}), \\ \tau \frac{dn}{dt} &= \sigma\left(n_\infty(V) - n\right), \\ \tau_S \frac{dS}{dt} &= S_\infty(V) - S \end{aligned} \tag{2·1}$$

with

$$\begin{aligned} I_{\mathrm{Ca}}(V) &= g_{\mathrm{Ca}} m_\infty(V)(V - V_{\mathrm{Ca}}), \\ I_{\mathrm{K}}(V,n) &= g_{\mathrm{K}} n (V - V_{\mathrm{K}}), \\ \omega_\infty &= \frac{1}{1 + \exp((V_\omega - V)/\Theta_\omega)}, \quad \omega = m, n, \text{ and } S. \end{aligned}$$

Here, V represents the membrane potential, n the opening probability of the potassium channels, and the variable S accounts for the presence of a slow dynamics in the system. I_{Ca} and I_{K} are the calcium and potassium currents, g_{Ca} and g_{K} the associated conductances, and V_{Ca} and V_{K} the respective Nernst potentials. $k_S = \tau/\tau_S$ defines the ratio of the time constants for the fast (V and n) and slow (S) dynamics. With parameter values as listed in Fig. 1, this ratio is quite small, and the model is numerically stiff.

Figure 1 shows a bifurcation diagram for the single-cell model with V_S as control parameter. We note the period-doubling cascade leading to chaos with periodic windows as V_S is reduced below -37.9 mV. As V_S is further reduced, a reverse period-doubling cascade leads to a state of periodic bursting with 5 spikes per burst around $V_S = -39.0$ mV. The interval of periodic bursting terminates in a saddle-node bifurcation leading to type-I intermittency and chaos before a periodic state with 4 spikes per burst is established through a new backwards period-doubling cascade.

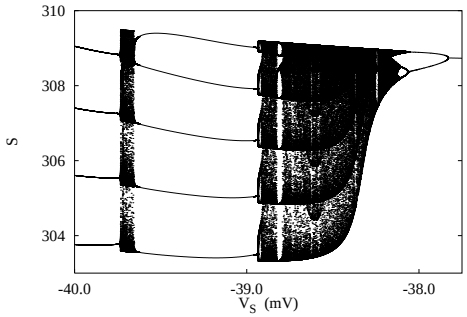

Fig. 1. Brute force bifurcation diagram for the individual β-cell. The model exhibits chaotic dynamics in the transition intervals between continuous spiking and bursting and between the main states of periodic bursting. $k_S = 0.57 \cdot 10^{-3}$. Model parameter values: $\tau = 0.02$s, $\tau_S = 35$s, $g_{\mathrm{Ca}} = 3.6$, $g_{\mathrm{K}} = 10.0$, $g_S = 4.0$, $V_{\mathrm{Ca}} = 25$ mV, $V_{\mathrm{K}} = -75$ mV, $V_m = -20$ mV, $V_n = -16$ mV , $\Theta_m = 12$ mV, $\Theta_n = 5.6$ mV , $\Theta_S = 10$ mV and $\sigma = 0.85$.

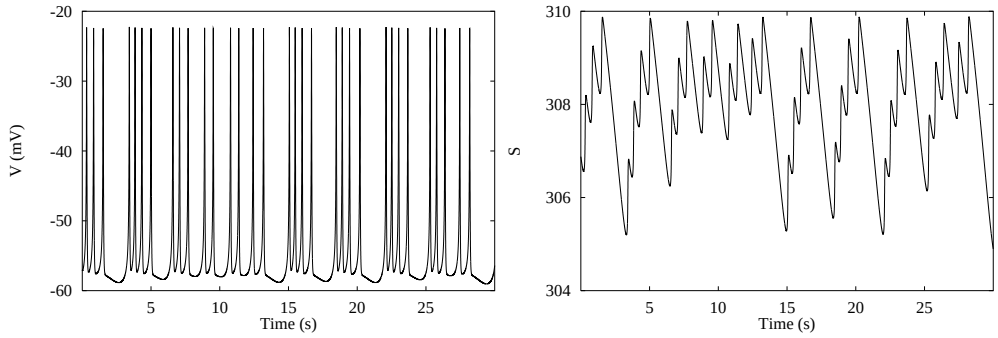

Fig. 2. Example of the temporal variations of the membrane potential $V(t)$, and of the slow variable $S(t)$ that controls the switching between the active and the silent phases. $V_S = -38.34$ mV. $S(t)$ has been multiplied by the factor τ_S/τ.

Figure 2 shows an example of the temporal variations of the variables V and S in the chaotic state existing for $V_S = -38.34$ mV. We notice the bursts in the membrane potential, consisting of different numbers of spikes. During each spike the slow variable increases a little until it reaches a threshold value, whereafter the cell switches into the silent phase.

To get a more complete picture of the bifurcation structure of the single-cell model, we have applied a brute force scanning approach to identify the main periodic solutions (up to period-20) and to locate and classify the associated bifurcations in the (k_S, V_S) parameter plane. Results of this study are displayed in Fig. 3. Here we observe an interesting squid-like structure for the chaotic regime with arms delineated by period-doubling cascades on one side and by saddle-node bifurcations on the other. Each arm separates a periodic bursting region with n spikes per burst from a region with n+1 spikes per burst. The number of spikes per burst seems to go to infinity as k_S approaches zero. The whole structure is surrounded by a PD^{1-2} curve at which the first period-doubling takes place. In the lower left corner of Fig. 3 we observe a so-called period-adding structure. [6] When crossing the curves of this

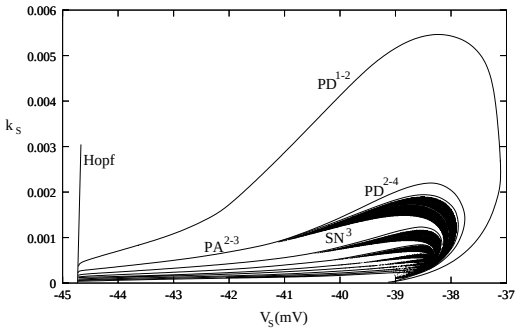

Fig. 3. Two-dimensional bifurcation diagram outlining the main bifurcation structure of the single cell model in the (V_S, k_S) parameter plane. Black points indicate chaotic solutions (including less pronounced periodic windows).

structure, a periodic bursting state with n spikes per burst is transformed into a state with $n+1$ spikes per burst. It is often assumed that this transition takes place in a continuous manner. However, at least in the present case the transition involves a set of bifurcations in which a stable n-spike solution disappears in a subcritical period-doubling bifurcation and a pair of node and saddle $n+1$-spike solutions are born. A preliminary investigation of the transition from the squid arms to the period-adding structure shows that there is an intermediate interval where the scenario involves a subcritical period-doubling and the emergence of type-III intermittency.

§3. Coupled chaotically spiking cells

A system of two coupled identical β-cells may be defined through the equations

$$\dot{\boldsymbol{x}} = \boldsymbol{f}(\boldsymbol{x}) + \boldsymbol{C}(\boldsymbol{y} - \boldsymbol{x}),$$
$$\dot{\boldsymbol{y}} = \boldsymbol{f}(\boldsymbol{y}) + \boldsymbol{C}(\boldsymbol{x} - \boldsymbol{y}),$$

where $\boldsymbol{f}(\boldsymbol{x})$, $\boldsymbol{f}(\boldsymbol{y})$ with $\boldsymbol{x} = (V_1, n_1, S_1)^T$ and $\boldsymbol{y} = (V_2, n_2, S_2)^T$ represent the dynamics of the individual cells in accordance with Eqs. (2·1). $\boldsymbol{C}$ is the coupling matrix for which we shall assume the form $\boldsymbol{C} = \mathrm{diag}(d_1, 0, d_3)$, indicating that coupling takes place between the fast (V_1 and V_2) and between the slow (S_1 and S_2) variables. The two components of the coupling may be considered to represent a resistive current driven by the difference in membrane potentials between the interacting cells, and a diffusive current driven by the differences in calcium concentration, respectively. In the following we shall assume that $V_S = -38.34$ mV with all other parameter values as stated in the caption to Fig. 1. With these parameter values the single-cell model operates in the chaotic regime with a positive value of the largest Lyapunov exponent. Figure 4 shows a bifurcation diagram for the coupled cell system in the two-parameter coupling plane. Here the curves delineate the regions in which the low periodic saddle cycles embedded in the synchronized chaotic state are transversely stable. The region of stability is to the upper right where the coupling is positive and sufficiently strong. When crossing the curves, transverse destabilization of the periodic cycles occurs via a pitchfork bifurcation (denoted **PF**), via a period-doubling

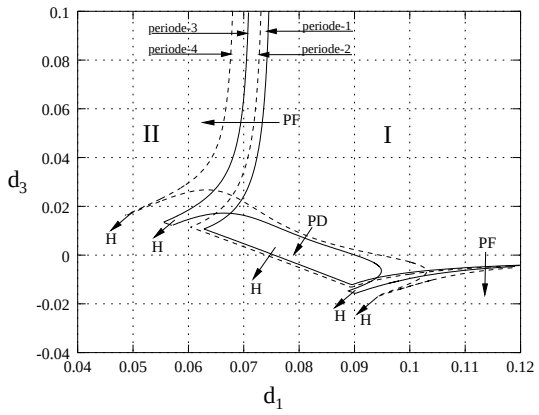

Fig. 4. Phase diagram showing the curves in two-parameter coupling space where some of the low-periodic cycles embedded in the synchronized chaotic state lose their transverse stability. **PF** denotes a pitchfork bifurcation, **PD** a period-doubling bifurcation, and **H** a Hopf bifurcation.

bifurcation (indicated as **PD**), or via a transverse Hopf bifurcation (**H**).

Each of the transverse bifurcations may be either sub- or supercritical. [17),18)] In a subcritical pitchfork bifurcation, two mutually symmetric doubly unstable saddle cycles will be situated on either side of the symmetric singly unstable saddle cycle embedded in the synchronized chaotic state before the bifurcation. As the point of destabilization is approached, the asynchronous cycles move closer to the symmetric saddle cycle to finally annihilate with it and leave a doubly unstable saddle cycle in the synchronization manifold. The unstable manifold of this cycle often stretches all the way to infinity, allowing trajectories starting near the synchronization manifold to diverge, if they happen to pass close to the transversely unstable periodic cycle. By virtue of the transitivity of the chaotic state, many trajectories will do so, and this produces an observable (i.e., global) riddling of the basin of attraction for the synchronized chaotic state. An analogous description applies for a subcritical period-doubling bifurcation.

In a supercritical transverse pitchfork bifurcation, two mutually symmetric singly unstable saddle cycles will exist around the destabilized low-periodic orbit right after the bifurcation. The unstable manifolds of these cycles will wrap around the synchronized chaotic state, and in this way trajectories starting near the synchronization manifold will often be restrained from reaching other asymptotic states or diverge to infinity. Hence, in this case we may observe the phenomena of local riddling, attractor bubbling and on-off intermittency.

The parameter region of interest in connection with a study of locally and globally riddled basins of attraction is the region where the first low-periodic cycle has become transversely unstable while the synchronized chaotic set is still stable on the average. The region of the coupling parameters where the synchronized chaotic state is attracting on the average is delineated by the blowout bifurcation curve. This curve is drawn in Fig. 5 as a heavy line. The riddling transition takes place via a pitchfork bifurcation of the period-1 saddle cycle along the branches I and III and via a period-doubling bifurcation of the period-4 saddle at branch II.

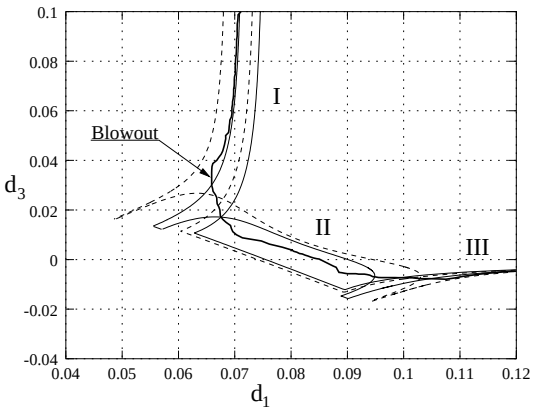

Fig. 5. Same bifurcation diagram as in Fig. 4, only the curve that marks the blowout bifurcation has also been drawn. Riddling of the basin of attraction for the synchronized chaotic state occurs in the region between the first transverse destabilization of a periodic cycle and the blowout bifurcation.

§4. Locally riddled basins of attraction

In the case of a locally riddled basin of attraction, almost all initial conditions eventually end up in the synchronized chaotic state. However, close to the synchronized state there is a dense set of repelling tongues. Hence, some trajectories make a large excursion in phase space before they are attracted to the synchronized chaotic state, while others never move far away from the synchronization manifold. Figures 6(a) and (b) display typical phase plots for the two types of behavior. These phase plots were obtained at coupling parameter values $d_1 = 0.067$ and $d_3 = 0.03$, where both the period-1 and the period-2 cycle are transversely unstable. The presence of a restraining mechanism produces a trapping zone around the synchronized chaotic state. Hence, the basin of attraction is locally riddled only, and the phenomenon observed in Fig. 6(b) is an illustration of attractor bubbling. If the coupling parameter d_1 is reduced to $d_1 = 0.063$ while d_3 is maintained at $d_3 = 0.030$, we have crossed the blowout bifurcation curve in the bifurcation diagram of Fig. 5. Now, the synchronized state is no longer attracting on the average. However, a trapping region still exists, and as a result we can observe the phenomenon of on-off intermittency. This is illustrated by the phase space trajectory of Fig. 7(a) and the corresponding temporal variation in Fig. 7(b). Here, we can observe how the system exhibits laminar (or off) phases of varying lengths in which the membrane potentials of the two β-cells exhibit synchronized chaotic oscillations, interrupted by relatively short turbulent (or on) phases where the cells move out of synchrony. Decreasing the coupling parameter d_1, we find that the average length of the laminar phases decreases as we move further away from the blowout bifurcation.

Let us separate the system variables into variables that describe the motions in the longitudinal subspace $\boldsymbol{\eta} = \boldsymbol{y} + \boldsymbol{x}$ and in the transverse subspace $\boldsymbol{\xi} = \boldsymbol{y} - \boldsymbol{x}$, respectively. In order to visualize the structure of the locally riddled basins of attraction we have performed an integration $\int_0^T |\boldsymbol{\xi}| dt$ of the synchronization error, from the

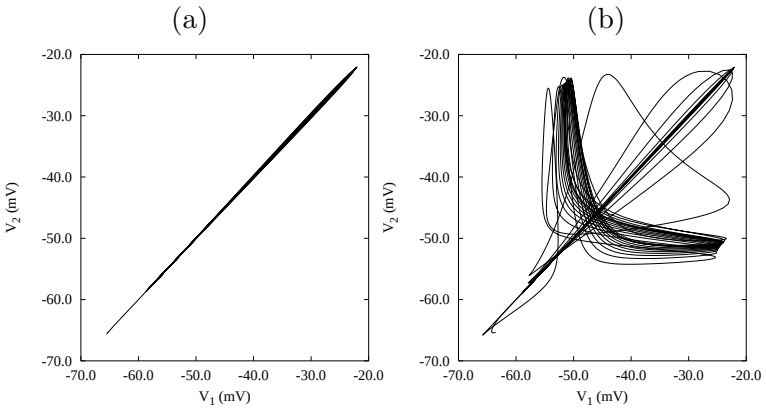

Fig. 6. Attractor bubbling. (a) and (b) display typical trajectories observed for $d_1 = 0.067$ and $d_3 = 0.030$ (i.e., near branch I in Fig. 5). In (a) the trajectory is almost immediately absorbed by the synchronized chaotic state. In (b) the trajectory first performs a major excursion in phase space.

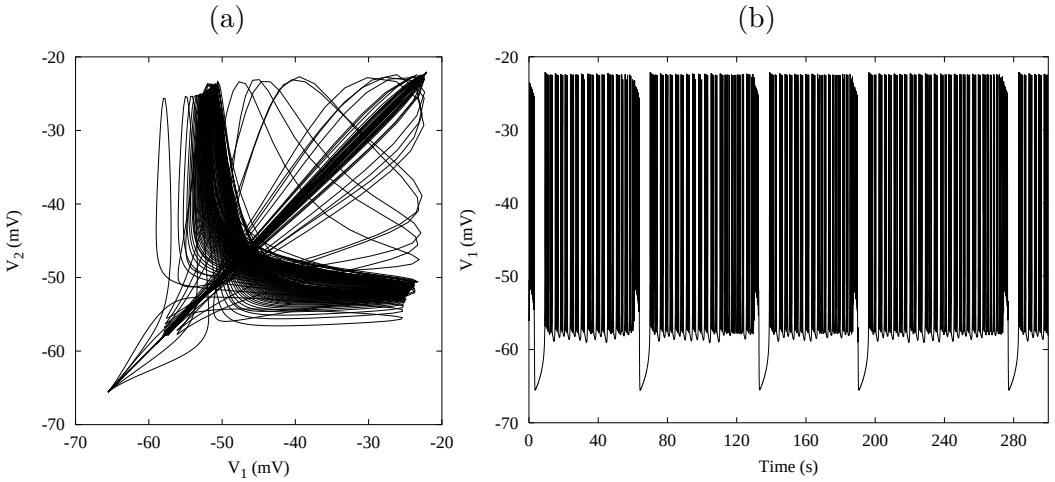

Fig. 7. On-off intermittency for $d_1 = 0.063$ and $d_3 = 0.030$. The synchronized chaotic state has lost its average attraction. (a) Phase space trajectory and (b) corresponding temporal variation of the membrane potential V_1.

initial state to a time T where final attraction to the synchronous state is realized. This provides a clear distinction between trajectories that are attracted almost immediately to the synchronized chaotic state (Fig. 6(a)) and trajectories that, while finally being attracted to the synchronized state, first perform a significant burst into phase space (Fig. 6(b)).

Figure 8 shows a cross section of the basin of attraction for $\xi_2 = \xi_3 = 0.0$, $\eta_2 = 0.02$ and $\eta_3 = 616.0$ for coupling parameter values $d_1 = 0.070$ and $d_3 = 0.030$. At these values only the synchronized period-1 cycle is transversely unstable. Initial conditions from which the trajectories are immediately attracted to the synchronized chaotic state are shown in black, and initial conditions from which the trajectory first makes a major excursion into phase space are left blank. Although the tongues are

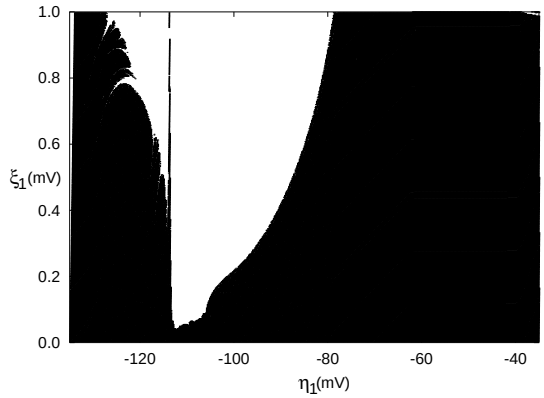

Fig. 8. Structure of the locally riddled basin of attraction for $d_1 = 0.070$ and $d_3 = 0.030$. Initial conditions from which the trajectories are almost immediately attracted to the synchronized chaotic state are shown in black.

extremely narrow, there is a dense set of locally repelling tongues (most pronounced in the left side) emanating from the chaotic set in the synchronization manifold ($\xi_1 = 0$).

Figures 9(a) and (b) illustrate how a bubbling excursion is initiated. Here we have plotted the temporal variation and the corresponding phase plot for a trajectory starting in one of the tongues of Fig. 8 (initial conditions are $\eta_1 = -125$ mV and $\xi_1 = 0.78$ mV). The temporal behavior shows how the nearly synchronized membrane potentials, after approximately 8s, reach a motion close to the unstable period-1 cycle. Since trajectories entering the proximity of the transverse unstable period-1 cycle are repelled, the coupled cells are lead into the very different asynchronous bubbling phase. The phase plot illustrates the relatively long period of time that the system spends in the neighborhood of the period-1 cycle before it bursts away from synchrony.

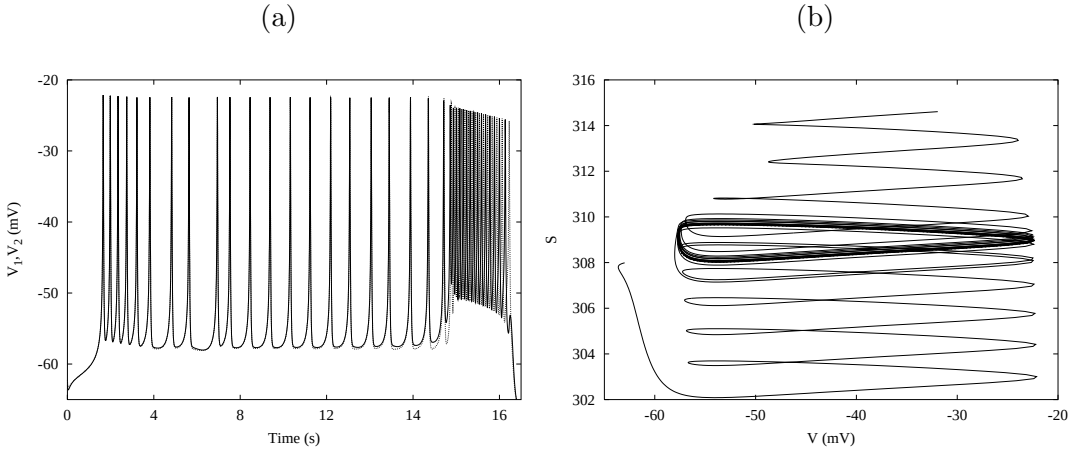

Fig. 9. Temporal variation (a) and phase space projection (b) of a trajectory that starts in the white area of Fig. 8. We observe how the trajectory approaches the unstable period-1 cycle in the synchronization manifold and then bursts away.

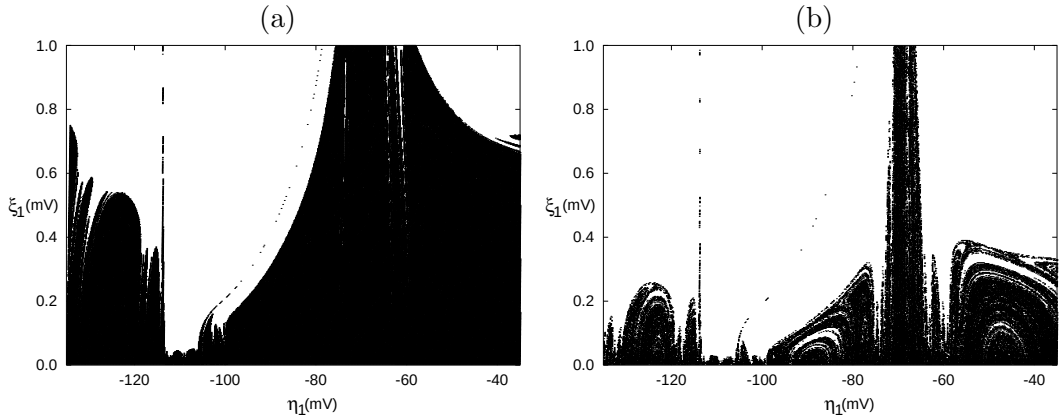

Fig. 10. Variation in the structure of the locally riddled basin of attraction as the coupling parameter is reduced. (a) $d_1 = 0.069$ and (b) $d_1 = 0.067$. We observe how the riddling structure becomes more and more apparent.

Figures 10(a) and (b) illustrate the changes in the structure of the locally riddled basin of attraction that occur as the system approaches the point of blowout. Here d_3 is maintained constant at $d_3 = 0.030$ while d_1 is gradually reduced. In Fig. 10(a), $d_1 = 0.069$, and the period-2 cycle has now become transversely unstable as well, resulting in a new set of tongues. If one follows a trajectory starting from one of these newly formed tongues, for instance from $\eta_1 = -62$ mV and $\xi_1 = 0.98$ mV, one can observe how it approaches the unstable period-2 cycle and moves in the neighborhood of this cycle for a while, before the trajectory is repelled and the cells move into an asynchronous bubbling dynamics. As compared with Fig. 8, the riddled basin structure in Fig. 10(a) is considerably more pronounced. Figure 10(b) shows the structure of the locally riddled basin for $d_1 = 0.067$. For $d_1 = 0.066$, i.e., right before the blowout bifurcation, the measure of initial conditions in the neighborhood of the synchronized chaotic state for which the trajectories are immediately attracted is quite small.

§5. Globally riddled basins of attraction

In accordance with our discussion in §3, the presence of a locally riddled basin of attraction is likely to be associated with a supercritical riddling bifurcation. Globally riddled basins of attraction can arise either directly after a subcritical riddling bifurcation or after a supercritical riddling bifurcation followed by a global bifurcation in which the trapping zone disappears in a contact crisis with the basin boundary, and the locally riddled basin of attraction is transformed into a globally riddled basin. A third scenario for the emergence of globally riddled basins of attraction involves the stabilization of saddle cycles away from the synchronization manifold. [17] All of these scenarios have been described in detail for a system of two coupled logistic maps, [17] and similar scenarios occur in our model of two coupled β-cells. Let us start by considering the structure near branch II in Fig. 5 where the synchronized period-4 cycle is first to lose its transverse stability, and where the destabilization occurs via

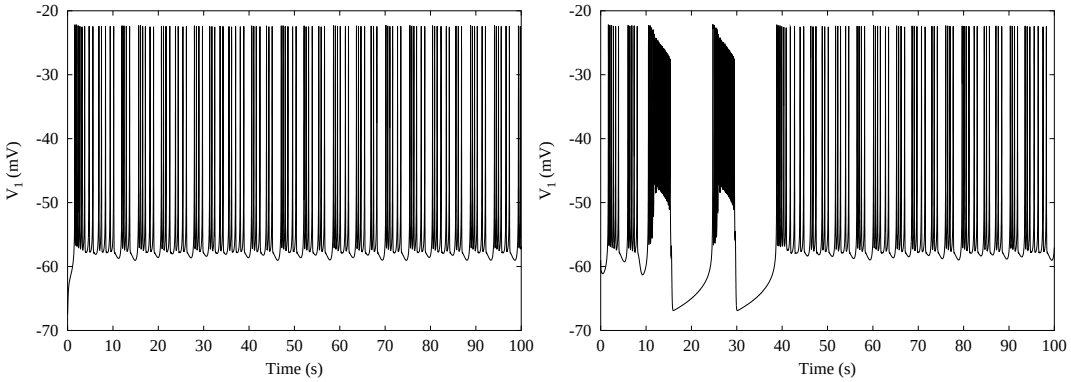

Fig. 11. Temporal variation of the membrane potential V_1 for two different initial conditions with $d_1 = 0.090$ and $d_3 = 0.0025$, i.e., near branch II in Fig. 5 where the symmetric period-4 cycle has undergone a transverse period-doubling bifurcation.

a period-doubling bifurcation. For $d_1 = 0.090$ and $d_3 = 0.0025$ we again observe a locally riddled basin of attraction. In spite of the dense set of repelling tongues issued from the synchronized chaotic state, almost all trajectories starting in the neighborhood of this state sooner or later end up being attracted to it. However, the trajectories can perform several bursts away from synchrony before the attraction materializes. This is illustrated in Fig. 11, where we have plotted a typical temporal variation of the membrane potential for two different initial conditions near the synchronized state. In the left panel of Fig. 11, the chaotically spiking cells synchronize almost immediately. In the other panel, a couple of excursions into phase space must be completed before synchronization is achieved. For some initial conditions, five or more such bubbling excursions are observed. Using the integrated synchronization error to distinguish differences in the temporal desynchronization, we have observed well defined regions in which all initial conditions experience one, two, three, four and five or more bursts out of synchrony before they obtain full synchronization. These regions appear to be confined by the manifolds of the transversely stable synchronous saddle cycles.

As d_3 is further reduced we observe a transformation from locally to globally riddled basins. This transformation is due to the appearance of a new attractor, emerging through stabilization of a saddle cycle outside the synchronization manifold, but within the trapping zone. At coupling parameter values $(d_1, d_3) = (0.09, 0.00125)$, this attractor is periodic with a temporal variation as shown in Fig. 12(a) and the corresponding phase space projection in Fig. 12(b).

Further reduction of the parameter d_3 causes the asymmetric periodic solution to go through a series of bifurcations resulting in the formation of an asynchronous chaotic attractor. Trajectories attracted by this limiting set investigate a much larger region of phase space, as seen in Fig. 13, with a typical temporal variation as illustrated in Figs. 14(a) and (b).

Between the coupling parameter values $d_3 = -0.00125$ and $d_3 = -0.0025$ a global bifurcation (boundary crisis) takes place. After this crisis the asynchronous

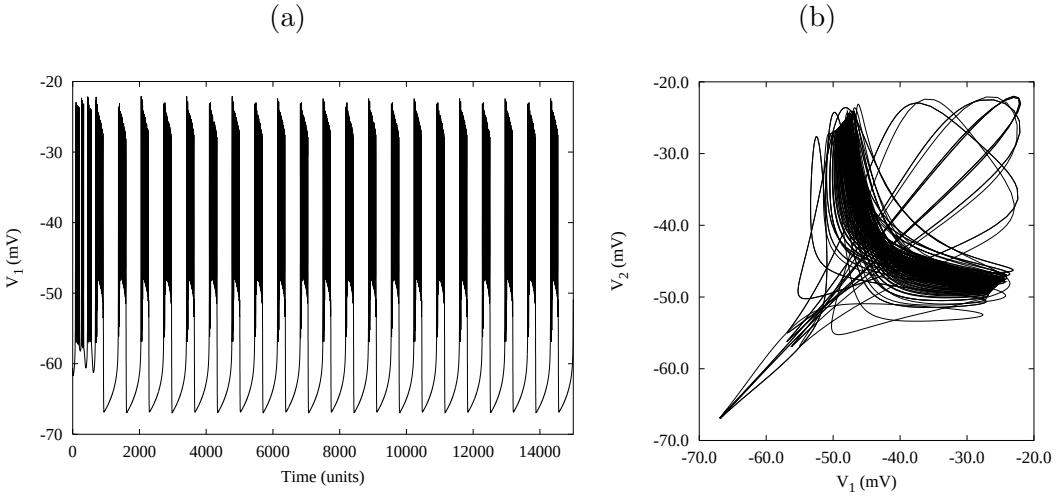

Fig. 12. Temporal variation (a) and phase space projection (b) of a trajectory attracted by the periodic asymmetric attractor at parameter values $(d_1, d_3) = (0.09, 0.00125)$. The attractor has appeared as a result of the stabilization of a saddle cycle outside the synchronization manifold.

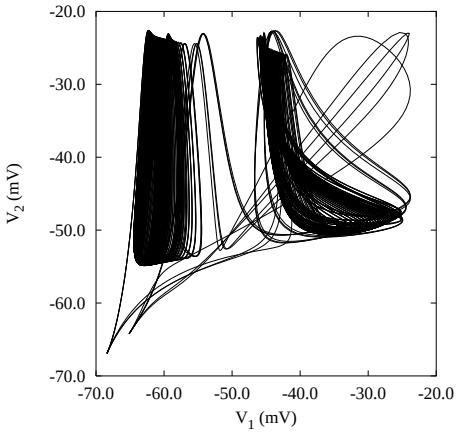

Fig. 13. Phase space projection of a trajectory attracted by one of the asynchronous chaotic states at $(d_1, d_3) = (0.09, -0.00125)$.

attractor has disappeared and trajectories not attracted by the synchronous chaotic state will diverge to infinity. These transitions all occur before the point of blowout is reached.

In other parts of the bifurcation diagram in Fig. 5, we observe a different scenario for the emergence of global riddling. Along branch III of the riddling bifurcation curve, the transverse pitchfork bifurcation of the symmetric period-1 cycle appears to be subcritical, and the riddling bifurcation directly leads to a globally riddled basin of attraction. Figure 15 shows a cross section of this basin for $d_1 = 0.104$ and $d_3 = -0.0065$. Here black points denote initial conditions from which the two cells attain complete synchronization, and white points represent initial conditions from which the trajectories diverge to infinity.

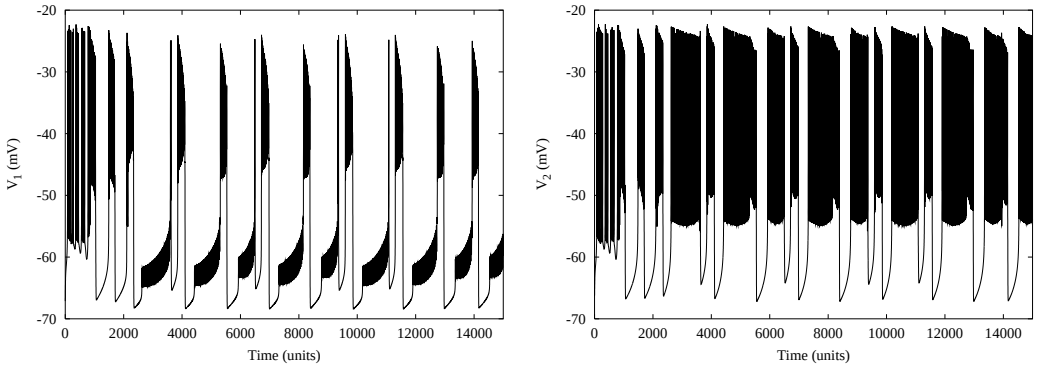

Fig. 14. Temporal variation of the membrane potentials for the two coupled cells for $d_1 = 0.090$ and $d_3 = -0.00125$. The basin of attraction is globally riddled, and many trajectories escape synchronization and approach an asynchronous chaotic state.

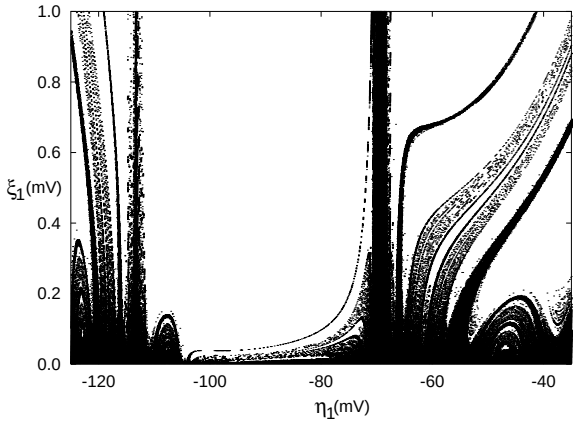

Fig. 15. Cross section of the globally riddled basin that exists for $d_1 = 0.104$ and $d_3 = -0.0065$. Here, black points denote initial conditions from which the two cells synchronize. Trajectories starting in white points diverge to infinity.

§6. Discussion

In the first part of our analysis we considered a number of bifurcation phenomena for the single-cell model. This study revealed the existence of a squid-formed region of chaotic dynamics in parameter space with a bifurcation structure of the individual arm typically consisting of a period-doubling cascade to chaos on one side and a saddle node bifurcation on the other. It also revealed that the so-called period-adding transitions between different bursting states can have an underlying and perhaps quite complicated structure.

The second part of our investigation revealed that a model of two coupled chaotically spiking and identical β-cells can exhibit a variety of different sub- and supercritical riddling bifurcations, including transverse pitchfork and period-doubling bifurcations. We illustrated the structure of the locally riddled basin of attraction that

one can observe immediately after a supercritical riddling bifurcation and described three different scenarios for the formation of globally riddled basins of attraction. Global riddling was observed directly after a subcritical riddling bifurcation, and in the case of a supercritical riddling bifurcation we observed how the locally riddled basin was transformed into a globally riddled basin either as an asynchronous saddle cycle gained stability resulting in the formation of a new attractor outside the synchronization manifold, or by virtue of a crisis bifurcation of the trapping zone.

References

1) R. M. Santos, L. M. Rosario, A. Nadal, J. Garcia-Sancho, B. Soria and M. Valdeolmillos, Eu. J. Physiol. (Pfluegers Archiv) **418** (1991), 417.
2) A. Sherman and J. Rinzel, Biophys. **59** (1991), 547.
3) A. Sherman, Math. Biol. **56** (1994), 811.
4) G. de Vries, A Sherman and H.-R. Zhu, Bull. Math. Biol. **60** (1998), 1167.
5) T. R. Chay, Physica **D16** (1985), 233.
6) Y.-S. Fan and T. R. Chay, Biol. Cybern. **71** (1994), 417.
7) H. Fujisaka and T. Yamada, Prog. Theor. Phys. **69** (1983), 32
8) A. S. Pikovsky, Z. Phys. **B55** (1984), 149.
9) K. Pyragas, Phys. Lett. **A181** (1993), 203.
10) K. Kaneko, Physica **D41** (1990), 137.
11) J. C. Alexander, J. A. Yorke, Z. You and I. Kan, Int. J. Bifurcation Chaos **2** (1992), 795.
12) E. Ott and J. C. Sommerer, Phys. Lett. **A188** (1994), 39.
13) P. Ashwin, J. Buescu and I. Stewart, Phys. Lett. **A193** (1994), 126.
14) L. Yu, E. Ott and Q. Chen, Physica **D53** (1992), 102.
15) N. Platt, E. A. Spiegel and C. Tresser, Phys. Rev. Lett. **70** (1993), 279.
16) Yu. L. Maistrenko, V. L. Maistrenko, A. Popovich and E. Mosekilde, Phys. Rev. **E57** (1998), 2713.
17) Yu. L. Maistrenko, V. L. Maistrenko, O. Popovych and E. Mosekilde, Phys. Rev. **E60** (1999), 2817.
18) Yu. L. Maistrenko, V. L. Maistrenko, O. Popovych and E. Mosekilde, Phys. Lett. **A262** (1999), 355.
19) S. Yanchuk, Y. Maistrenko, B. Lading and E. Mosekilde, Int. J. Bifurcation Chaos, to appear.
20) N. F. Rul'kov, L. S. Tsimring and H. D. I. Abarbanel, Phys. Rev. **E50** (1995), 314.
21) G. A. Johnson, D. J. Mar, T. L. Carroll and L. M. Pecora, Phys. Rev. Lett. **80** (1998), 3956.
22) M. G. Rosenblum, A. S. Pikovsky and J. Kurths, IEEE Trans. CS **44** (1997), 874.
23) V. Astrakov, M. Hasler, T. Kapitaniak, A. Shabunin and V. Anishchenko, Phys. Rev. **E58** (1998), 5620.
24) C. Mira, L. Gardini, A. Barugola and J.-C. Cathala, *Chaotic Dynamics in Two-Dimensional Noninvertible Maps* (World Scientific, Singapore, 1996).
25) A. L. Hodgkin and A. F. Huxley, J. Physiol. Lond. **117** (1952), 2050.